JOURNAL OF PROPULSION AND POWER
Vol. 19, No. 5, September–October 2003

Partial Fuel Filling in Pulse Detonation Engines

Chiping Li* and K. Kailasanath†
U.S. Naval Research Laboratory, Washington, D.C. 20375

Partial fuel filling in pulse detonation engines (PDEs) is a fuel-filling strategy in which only a part of the PDE tube is filled with a combustible mixture and the rest of the tube with a nonreactive mixture. The structures of the pressure waves in the flowfield in partially filled PDEs are illustrated in detail by systematic numerical simulations. The simulations show those pressure waves control the development of the flowfield and, hence, the thrust production of the PDE. Based on the pressure information from the simulations, performance analysis is also conducted. The analysis shows that for a fuel section of a given length the impulse increases with the length of the nonreactive section, eventually approaching an asymptotic value. Hence, the partial fuel filling in a PDE increases the fuel-based specific impulse I_{sp}^{f}, which represents an improvement in the fuel efficiency for air-breathing applications, similar to the benefit generated by the bypass air introduced in gas-turbine jet engines. However, it does carry a penalty of reducing the total-mixture-based specific impulse I_{sp}^{m} because less chemical energy is contained per unit volume. As a consequence, the total engine output from a PDE partially filled with the combustible mixture is lower compared to that from one fully filled with the combustible mixture. Lower I_{sp}^{m} also implies reduction in fuel efficiency for PDE rocket applications.

Introduction

DETONATION is a very efficient combustion process that couples the energy release in combustion to shock waves, generating extremely high pressures directly from the combustion process. A pulse detonation engine (PDE) is a propulsion device using the high pressure generated by repetitive detonation waves in a combustible mixture. The PDE concept was explained in detail in Refs. 1–3. Past and more recent developments in the PDE research were summarized in Refs. 4 and 5. The thrust producing part of a PDE can be idealized as a tube, that is, the thrust tube, filled with a detonable mixture, as shown in Fig. 1a. A typical PDE operating cycle can be summarized as follows: 1) filling the PDE tube with a detonable mixture, 2) initiating detonation waves in the mixture and completing the combustion of the mixture in the PDE tube in the form of detonation, and 3) evacuating the PDE tube for refilling the tube. Figure 1a also shows that a detonation is initiated near the end wall and propagates toward the tube exit. The end wall, (the thrust wall) receives the high pressure generated in the detonation combustion process to produce thrust. In the case of a converging or diverging thrust tube, the pressure on the converging or diverging part of the tube also contributes to the thrust production either positively or negatively, depending on the orientation of that part of the tube wall.

In PDE operation, the thrust tube does not need to be completely filled with fuel. Actually, partial fuel filling can have some significant benefits. Figure 1b shows a schematic of a partially filled PDE thrust tube. In contrast to the thrust tube shown in Fig. 1a, which is completely filled with a detonable mixture, only a portion of the thrust tube next to the thrust wall is filled with a detonable mixture, and the rest of tube is filled with a noncombustible mixture such as air. In a fully fueled thrust tube, the detonation travels through the entire tube and exits through the open end with its full strength. As the detonation exits the tube, a sizable portion of the converted chemical energy in the high-pressure region traveling along with the detonation is lost. In the partially filled tube, the detonation is quenched at the interface between the combustible and noncombustible sections, degenerating into a nonreactive shock. Without the high-pressure support from the detonation process, the shock strength gradually reduces as it travels through the rest of the tube. The noncombustible section helps to retain the high pressure generated by the detonation in the combustible section to produce more thrust after the detonation process ceases. When the shock reaches the tube exit, its strength is weaker than that of the detonation exiting a PDE thrust tube fully filled with the combustible mixture, resulting in less loss of the converted chemical energy. Therefore, the operation can have higher fuel efficiency. In addition to its positive impact on the PDE performance, the noncombustible section also can act as a buffer zone between two consecutive cycles, which helps to evacuate the burned product and to prevent premature combustion during the fuel refilling process. However, replacing a part of the combustible mixture by a noncombustible mixture does reduce total chemical energy available in the operation cycle, resulting in less total thrust output during the cycle. Also, because the shock speed in the inert section is lower than the detonation speed in the combustible section, the total cycle time is slightly longer, resulting in a somewhat lower operating frequency.

Different aspects of the partial fuel filling in PDEs have been studied analytically, numerically, and experimentally. Many of those past studies[6–13] are related to using nozzles or extension tubes to capture the otherwise lost converted chemical energy. The studies show that the PDE performance can be significantly affected by a nozzle. In most cases, the performance is enhanced. For example, the experiments by Zhdan et al.[6] showed that using a straight extension tube of length 7–10 times that of the fuel section resulted in an increase in impulse by a factor of about two. In a numerical study by Eidelman and Yang,[8] the effect of nozzles of different shapes filled with air on the impulse was explored. The simulations showed that a straight nozzle could lead to a significant increase in the impulse. Because the fuel amount remained the same for the different nozzles, an increase in impulse implies an increase in fuel efficiency. Therefore, the authors further concluded that nozzles could drastically increase the fuel efficiency of PDEs. Daniau et al.[13] demonstrated that the fuel efficiency was increased considerably by the presence of a nozzle in wide ranges of shape and length. More comprehensive reviews on the effect of nozzles may be found in the review paper by Kailasanath.[5]

There also have been studies[14–16] on the effect of fuel distribution inside the PDE tube and/or nozzle on the performance. Cambier and Tegner[14] simulated reactive flows in a PDE thrust tube with nozzles

Presented as Paper 2001-3933 at the AIAA/ASME/SAE/ASEE 37th Joint Propulsion Conference, Salt Lake City, UT, 8–11 July 2001 and Paper 2002-0610 at the AIAA 40th Aerospace Sciences Meeting, Reno, NV, 14–17 January 2002; received 18 June 2002; revision received 16 April 2003; accepted for publication 17 April 2003.

*Laboratory for Computational Physics and Fluid Dynamics. Associate Fellow AIAA.
†Laboratory for Computational Physics and Fluid Dynamics. Associate Fellow AIAA.

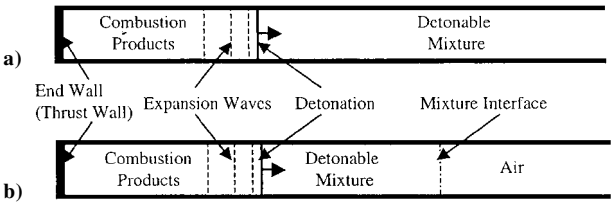

Fig. 1 Schematic of PDE thrust tubes with the detonable mixture a) fully filled and b) partially filled.

of different shapes. In the study, a fuel layer of different thickness was distributed along the walls of the thrust tube and the attached nozzle. The authors' original motivation was to enhance the PDE performance by placing the fuel and, therefore, the high-pressure region generated by the detonation near the wall. The study indeed showed that, as the fuel-layer thickness decreased the impulse reduced accordingly, but the fuel-based specific impulse I_{sp}^{f} increased significantly.

In an earlier study,[15] we used the time-accurate numerical simulation as a tool to study the development of the flowfield during a PDE cycle, from the initiation to times long after the detonation exits the tube. It was found that most of the thrust was produced after the detonation had exited the tube. The expansion waves generated at the tube exit play a particularly important role at this stage. In addition to the flow in a PDE tube fully filled with the combustible mixture, we also simulated the flow development in partially filled tubes. The results show that there are strong expansion waves generated at the interface between the combustible and nonreactive sections when the detonation passes through the interface. These interface expansion waves play an equally important role in thrust production. In Ref. 15, we showed that the end-wall pressure history is dominated by the interface expansion and exit expansion waves. The patterns in the pressure histories shown in Ref. 15 were later observed in the experiments[17,18] conduced at the Stanford University for a very different tube length and mixture conditions. Since then, we have conducted systematic simulations of the flow field in PDE tubes of different lengths with wide ranges of mixture and filling parameters. In this paper, based on these simulations, we will 1) illustrate the development of pressure waves during the PDE cycle, 2) explain important factors in thrust production, and 3) present performance trends for partially filled PDEs. First, we will briefly describe the numerical methods and physical models used in the simulations as well as validation of those models.

Physical Models and Numerical Methods

Physical Models

In the simulations, the conservation mass equation (1), momentum equation (2), energy equation (3), and individual species equation (4) were solved as follows:

$$\frac{\partial \rho}{\partial t} + \nabla \cdot \rho \boldsymbol{V} = \boldsymbol{0} \tag{1}$$

$$\frac{\partial \rho \boldsymbol{V}}{\partial t} + \nabla \cdot (\rho \boldsymbol{V}\boldsymbol{V} + P\boldsymbol{I}) = \boldsymbol{0} \tag{2}$$

$$\frac{\partial E}{\partial t} + \nabla \cdot [(E + P)\boldsymbol{I}]\boldsymbol{V} - \boldsymbol{q} = \boldsymbol{0} \tag{3}$$

$$\frac{\partial n_i}{\partial t} + \nabla \cdot n_i(\boldsymbol{V}) - \omega_i = \boldsymbol{0} \tag{4}$$

In Eqs. (1–4), ρ, $\boldsymbol{V}$, P, E, n_i, ω_i, and q are mass density, velocity, pressure, energy density, species number density, species production rate, and total energy conversion rate in the chemical reaction. Because we only consider a single PDE cycle, diffusive transport processes such as thermal conduction, molecular diffusion, thermal diffusion, viscosity, and radiation transport inside the flowfield are not included. For a continuous multicycle operation, the effect of cumulative heat transfer through the tube wall can be important, and therefore, the related processes need to be included. The convective part of the Eqs. (1–4) is numerically solved using the flux-corrected transport algorithm (FCT).[19] This algorithm is conservative, accurate, stable, and monotonic (positivity-preserving), where the monotonicity is achieved by introducing a diffusive flux and later correcting the calculated results with an antidiffusive flux modified by a flux limiter. A sample code based on the FCT algorithm may be found in Ref. 20.

In the simulations, the chemical reactions are represented by a two-step induction-parameter model.[21] In this model, the first step represents the induction process, in which combustion radicals are formed and represented by the induction parameter. Then, this induction parameter is convected as a species. The second step represents the recombination process, in which energy is released. The induction-time data, on which the induction parameter is based, were obtained from shock-tube experiments conducted at conditions applicable to the detonation regime.[22] The code used in this study consists of separate convection and chemistry modules. The different modules are coupled by a time-step splitting technique.[23] In the high-temperature and pressure conditions behind the detonation, the pressure is no longer a linear function of the internal energy. Therefore, the pressure and temperature cannot be explicitly calculated from the internal energy using the ideal gas law. In this study, we used seventh-order fits based on the enthalpy data in the JANNAF tables[24] to calculate the temperature and pressure iteratively.

Initial Conditions

The stoichiometric ethylene–oxygen mixture considered in most cases is highly energetic and readily detonable. Therefore, no additional fuel, hence, chemical energy, is needed to facilitate the initiation process. In all simulations, the detonation is initiated by a 10-mm section of the same mixture at an elevated pressure (4 atm) and temperature (1200 K) next to the end wall. In the initiation region, density of the mixture, and chemical energy content are the same as those in the rest of the detonable mixture region. For the much less energetic stoichiometric ethylene–air mixture, this 10-mm initiation zone is composed of the stoichiometric ethylene–oxygen mixture, but other conditions are the same (4 atm and 1200 K).

Grid Resolution

In this study, what we need is the overall flow development that yields sufficiently accurate pressure histories on the end wall, rather than detailed detonation cell structures. Therefore, relatively coarse grid systems can be used to save computational costs, as long as the main detonation features, such as detonation speed, pressure, and temperature distributions behind detonation, are grid-resolution independent. In our preliminary test, we used four grid resolutions, $dx = dy = 0.5$ mm, $dx = dy = 1.0$ mm, $dx = dy = 2.0$ mm, and $dx = dy = 5.0$ mm. When the first three resolutions are used, the computed detonation velocity is about 2370 m/s and the detonation pressure ratio is about 33. Both values are consistent with the prediction from the Gordon and McBride code.[25] Furthermore, in these three simulations, the overall property profiles behind the detonations are very similar. The fourth simulation, using $dx = dy = 5.0$ mm, shows a detonation velocity of 2650 m/s, which is significantly higher than the correct value for this mixture. Obviously, computational resolutions at this level are not adequate. In all of the important physical features to be resolved in the problem studied here, the detonation has the most stringent resolution requirement. Should a resolution be adequate for simulating the detonation, it is more than adequate for simulating other flow features such as the nonreactive shocks and expansion waves near the exit of the thrust tube. Therefore, the grid resolution of $dx = dy = 1.0$ mm is used in all of the simulations in this study.

Boundary Conditions and Computational Domains

In the simulations, one important issue is the boundary condition at the tube exit. In either fully or partially filled cases, before the detonation or nonreactive shock reaches the tube exit, the pressure value in the tube section ahead of the detonation is the same as the ambient value outside of the tube. After it exits the tube, the

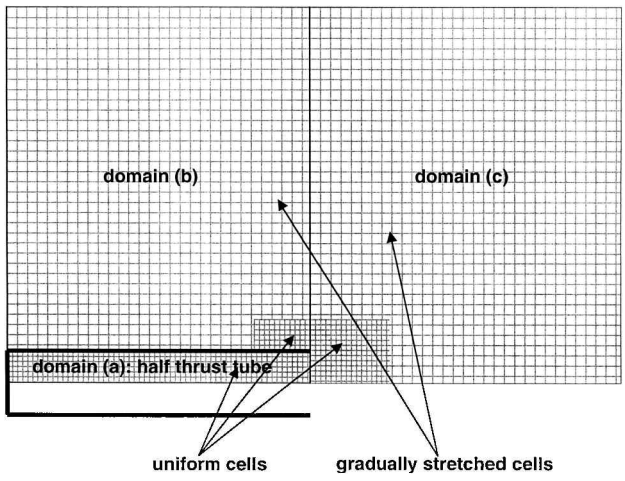

Fig. 2 Schematic of computational domains used in the simulations.

shock is still rather strong and continues to propagate outside the tube. In the region between the tube exit and the shock, the pressure becomes significantly higher than the original ambient value. As the shock propagates away from the tube exit, this pressure gradually decreases. Because the flow development in the PDE tube strongly depends on the pressure in the exit region outside the tube, the flow evolution in the exit region needs to be correctly simulated as part of the overall solution. Therefore, in simulations of this type, large computational domains must be used to cover the exit region and to avoid any influences from domain boundaries during the simulation.

The multiple computational domains are shown in Fig. 2. Domain a covers one-half of the two-dimensional channel representing the PDE thrust tube above the symmetry line. The width of the channel is 40 mm, and the length ranges from 100 to 5000 mm. In this domain, the computational cells are uniformly distributed, and the cell size is $dx = dy = 1.0$ mm. The grid in domain b is 500×500, representing an area of $19{,}877 \times 19{,}877$ mm^2 immediately above the thrust tube. In both the x and y directions, the first 250 cells from the thrust tube exit are uniformly distributed, and the cell size is 1.0 mm. Therefore, the size of the uniform region is 250×250 mm^2. Beyond the uniform region, the cells are stretched at a ratio of 1.025 in both directions. Domain c represents the region downstream from the tube exit, above the symmetry line of the tube. The grid in domain c is 500×520, and the actual domain area is $19{,}877 \times 19{,}697$ mm^2. The computational cells are uniformly distributed within the first 250 cells in the x direction and the first 270 cells in the y direction from the intersection of the tube exit and tube symmetry line. The size of the uniform region in domain b is 25×27 mm^2, and the corresponding cell size is 1.0 mm in each direction. From the 251st cell in the x direction and the 271st cell in the y direction, the computational cells then are stretched at a ratio of 1.025. The large stretched regions in domains b and c allow one to impose the boundary conditions at boundaries that are far away from the region where the flow undergoes rapid changes. In these large domains, the exited shock can propagate in the ambient environment without impinging on the boundary prematurely. Therefore, the flow in the region near the tube exit can develop properly. Using the large computational domains described, we are able to simulate systematically the long-term (more than 20 times of the residence time of the detonation in the thrust tube) development of the flow in the thrust tube and the exit region.

The top boundary of domain a and the bottom boundary of domain b are separated by the upper wall of the thrust tube. The right boundaries of domains a and b are connected to the left boundary of domain c. When the FCT algorithm is used, the numerical solution for every spatial point at a particular time step depends on its neighboring five grid points in each grid direction. Therefore, an overlapping region of 10 grid points is used to assure completely transparent connection between the right boundaries of domains a and b and the left boundary of domain c. In the simulations, a detonation is generated near the left end of domain a, and propagates right through domain a into domain c, and then domain b.

On the upper and left boundary of domain a, the reflective boundary condition is used to represent the end wall and sidewall of the PDE tube, respectively. On the lower boundary of domain a, the symmetric condition is used to represent the center, symmetry line of the PDE tube. The left boundary of domain c is connected to the right boundary of domain a (the tube exit) and the right boundary of domain b in the manner discussed earlier. On the other boundaries of domains b and c (far-away boundaries), the supersonic outflow condition is used. However, as already discussed, domains b and c are sufficiently large so that the simulated flow features do not reach those boundaries during the simulation. Near those boundaries, the flowfield remains quiescent at the ambient condition. Therefore, details of the boundary condition used on those boundaries are irrelevant as long as no additional flows are induced on the boundaries.

Pressure Waves in the PDE Flowfield

During a PDE cycle, the flowfield in a PDE thrust tube is highly transient and dominated by different types of moving pressure waves. These pressure waves control the evolution of the pressure distribution in the tube. Among the pressure waves, there are three most important ones: 1) the detonation, which is initiated at the end wall at the beginning of a PDE cycle; 2) the exit expansion waves, which are generated at the tube exit when and after the detonation or shock degenerated from the detonation exits the tube and propagate upstream toward the end wall; and (3) the interface expansion waves, which are generated at the material interface between the fuel and nonreactive sections when the detonation passes through the interface and propagate both downstream and upstream from the interface. In this section, we illustrate the development of those pressure waves based on results from the simulation for the following conditions. The length of the PDE thrust tube is 1350 mm and the mixture ratio of the detonable mixture is C_2H_4:O_2/1:3 (stoichiometric ethylene–oxygen mixture). The length of the fuel section is 1350 (100% fill), 1012 (75% fill), 675 (50% fill), and 337 mm (25% fill). In the partially filled cases, the rest of the tube is filled with air. After the detonation is initiated near the end wall, the detonation front quickly reaches a steady propagating state. There are many common features in the flow development in all of the cases. However, the material interface between the combustible and nonreactive section in the partially filled cases makes a significant difference in the flow development in the partially filled cases. We will present the fully filled case as the base case. In this case, only the detonation and exit expansion waves affect the flow development as the detonation propagates through the thrust tube into the surrounding regions. The tube length and mixture conditions used in this simulation are the same as that used in the experiment at Stanford University. Comparison between the simulation and the experiment will also be discussed in this section.

Flow Development in the Fully Filled Case

Figure 3 shows the pressure distributions in the thrust tube at different times as the detonation front propagates through the tube and long after the detonation has left the tube. Figure 4 presents the

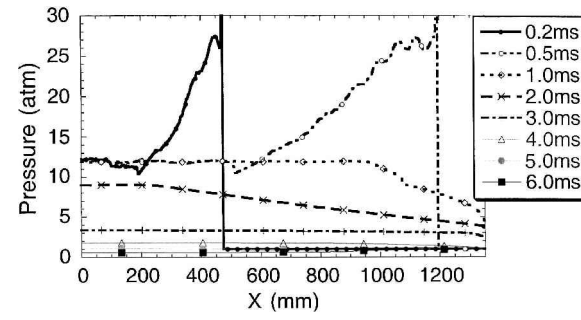

Fig. 3 Pressure distribution at different times in a 1350-mm tube completely filled with a stoichiometric C_2H_4/O_2 mixture.

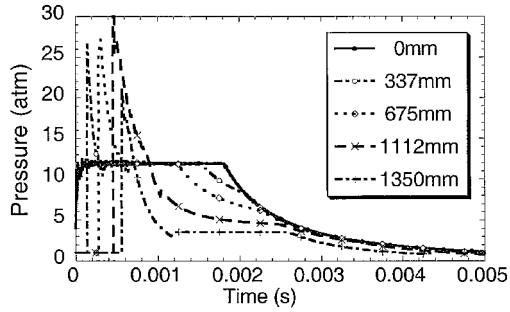

Fig. 4 Pressure histories at different locations in a 1350-mm tube completely filled with a stoichiometric C_2H_4/O_2 mixture.

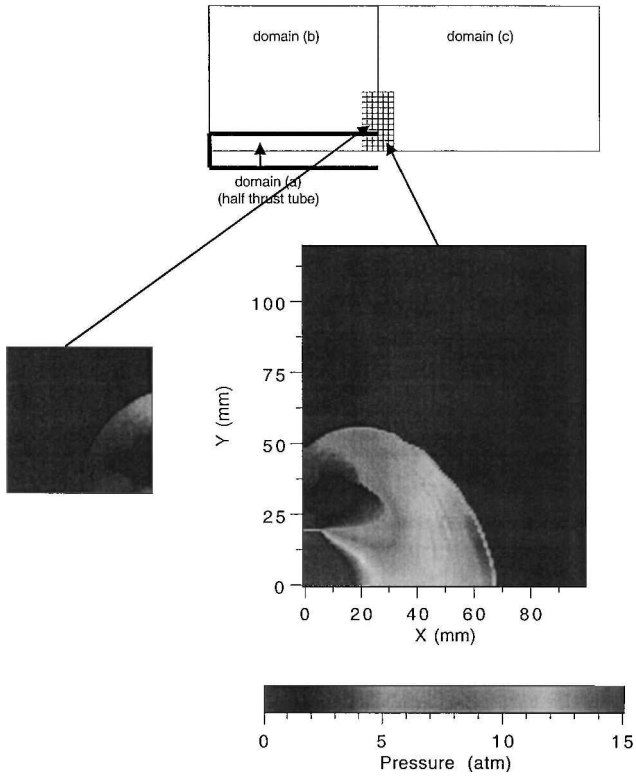

Fig. 5 Pressure near the exit of the thrust tube from domains a and c at 0.04 ms after detonation exits the tube in the fully filled case.

pressure histories at different locations. Figures 3 and 4 are complimentary and provide a clear picture of the flowfield development in the tube. At 0.2 ms, the detonation front is at approximately 470 mm from the end wall. At this time, there is an approximately 200-mm region near the head end, where the pressure value is flat at about 12 atm. At 0.5 ms, the detonation has traveled about 1200 mm, approaching the tube exit. The flat pressure region has extended to about 500 mm from the end wall.

The detonation front exits the thrust tube and enters the open environment, represented by computational domains b and c, at about 0.56 ms after initiation of the detonation near the end wall. After the detonation enters the ambient air in the open environment, the detonation is quenched and becomes a strong, nonreactive shock. Because of a large pressure gradient near the exit, expansion waves quickly develop in the nearby region, and the pressure behind the shock drops rapidly. The combustion products begin to exit rapidly from the thrust tube. Figure 5 shows the pressure distributions near the exit into domains b and c at 0.6 ms. At this time, the detonation has degenerated into a nonreactive shock, located at about 67 mm downstream from the tube exit. The pressure immediately behind the shock is slightly higher than 15 atm. Further behind the shock, along the axis, the pressure becomes lower (11 atm) through strong

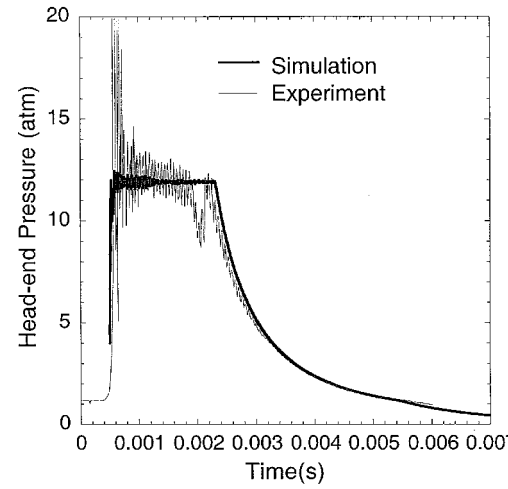

Fig. 6 Comparison of the end-wall pressure histories from the simulation and Stanford experiment[18] in the fully filled case.

expansion waves. At about 26 mm from the tube exit, there is another shock. Behind this shock, the pressure is about 23 atm, matching the pressure value inside the tube. Above the tube axis, the shock wave curves back, extending into domain b above the tube. It is clear that the pressure near the tube exit is significantly different from the ambient value.

After the detonation exits the tube, the pressure in the exit region gradually decreases, and expansion waves originating in the exit region gradually move upstream into the thrust tube at the local sound speed. However, at 1.0 ms after the detonation initiation, that is, 0.44 ms after the detonation exits the tube, the pressure value in a major part of the tube from the end wall still remains flat at about 12 atm (Fig. 3). This near constant pressure value in the tube maintains a similar pressure value on the end wall and results in strong thrust production for quite a long period. This is further confirmed by the plateau region in the pressure history on the end wall (0 mm) shown in Fig. 4. The pressure value on the end wall remains at about 12 atm until 1.9 ms, when the expansion waves from the tube exit reaches the end wall. After the expansion waves reach the end wall, the pressure in the tube gradually decreases, approaching the ambient value.

Figure 6 shows a comparison between the pressure histories from the simulation just discussed and the experiment conducted at Stanford University.[18] The two pressure histories are in good quantitative agreement. The initial spikes in the experimental data are most likely related to the particular initiation procedure used in the experiment. Also, the pressure plateau in the experimental curve is not as flat as that in our computed results. This is possibly due to the residual air existing near the tube exit.

Partially Filled Cases and Effects of the Material Interface

In the partially filled cases, there exist a material interface between the fuel and air sections. When the detonation reaches the nonreactive region, it is quenched and degenerates into a nonreactive shock. Because the shock suddenly loses the energy support from the chemical reaction, its strength reduces dramatically, and strong expansion waves are generated at the interface, reducing the pressure on both sides of the interface. However, unlike the case of detonation exiting the tube, the flow is still confined by the tube wall and the shock does not decay as quickly as in the preceding case. This effect actually helps to maintain the high pressure on the end wall, prolonging the thrust production, albeit at a lower level.

In this section, we will discuss the 50% filled case with some degree of detail to illustrate the effect of the material interface at the end of the detonable region. Figure 7 shows the pressure distributions at different times. Figure 8 shows pressure histories at different locations in the tube. At 0.2 ms, the detonation is at about 470 mm from the end wall, and the pressure distribution is identical to that at the same time in the fully filled case. This is not surprising

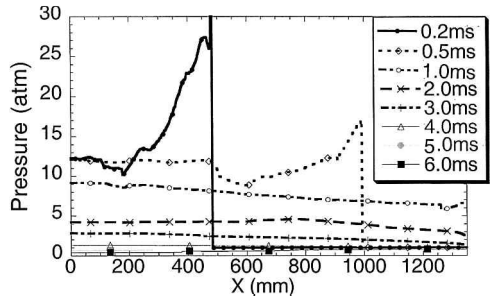

Fig. 7 Pressure distribution at different times in a 1350-mm tube with a half fill of a stoichimetric C_2H_4/O_2 mixture.

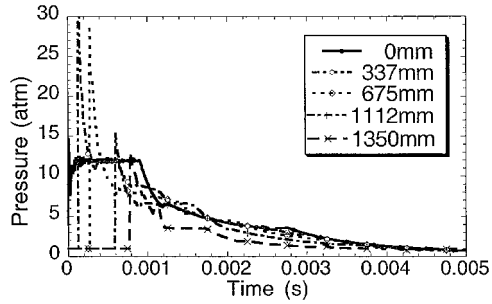

Fig. 8 Pressure histories at different locations in a 1350-mm tube with a half fill of a stoichiometric C_2H_4/O_2 mixture.

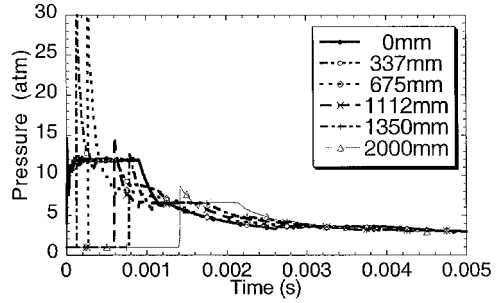

Fig. 9 Pressure histories at locations near the head end in a 5000-mm tube with a 675-mm fill of a stoichiometric C_2H_4/O_2 mixture.

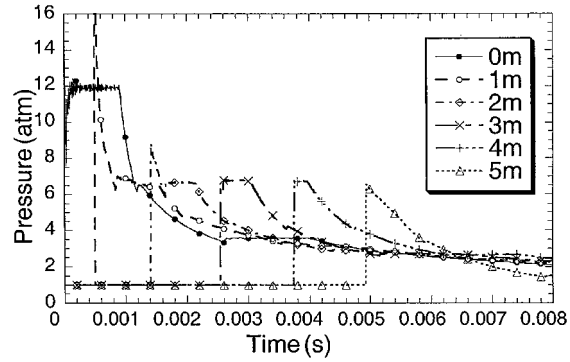

Fig. 10 Pressure histories at different tube locations in a 5000-mm tube with a 675-mm fill of a stoichiometric C_2H_4/O_2 mixture.

because the detonation travels through the exact same mixture. The detonation enters the nonreactive zone at about 0.23 ms and, then, degenerates into a nonreactive shock. At 0.5 ms, this shock travels 993 mm from the end wall. The peak pressure behind is about 17 atm, which is far lower than that behind the original detonation (above 30 atm). A low-pressure region can be observed behind the shock. This is due to the expansion waves generated when the detonation passes the interface. These expansion waves will propagate upstream, eroding the high pressure in the upstream region. The pressure history at the end wall shows that the interface expansion waves reach the end wall at about 0.97 ms, terminating the pressure plateau (Fig. 8). In this case, the length of the pressure plateau at the end wall is considerably shorter than that in the fully filled case, that is, 0.97 vs 1.9 ms. This difference can be attributed to the different times needed for the different expansion waves and the detonation to travel between the end wall and the tube exit. Also, the interface expansion waves result in a steeper decline in the end-wall pressure, after they reach the end wall. Furthermore, the pressure history at the tube exit (Fig. 8) shows the pressure peak representing the shock at the tube exit. In this case, the peak value at the exit is just above 10 atm, which is significantly lower than that in the fully filled case (23 atm) and represents much less loss in the mechanical energy.

In the pressure histories taken at the 75% tube length (1112 mm), a flat-pressure region at about 6.5 atm can be observed from 0.8 to 1.6 ms. A detailed analysis indicates that this feature occurs because the contact surface, pushing the material ahead of the detonated mixture, acts like a near-constant-velocity piston, until the interface wave reflects from the head wall and reaches the contact surface to reduce its velocity. In the 25% filled case, this interesting feature becomes more pronounced and can be seen in the pressure histories taken from any location from the middle point of the tube to approximately 85% of the tube length. This is because, in the 25% filled case, the interface expansion waves are generated earlier and have more time to influence the flow. Also, the pressure plateau at the end wall becomes even shorter (about 0.5 ms) than that in the 50% filled case. On the other hand, in the 75% filled case, the interface expansion waves arise much later, and the end-wall pressure plateau is also correspondingly longer.

In all partially filled cases presented, the influence of the interface expansion waves is eventually overtaken by that of the expansion waves generated at the tube exit when the shock exits the tube. To separate the effect of the interface expansion waves from that of the exit expansion waves, a simulation was conduced using a much longer tube (5000 mm) while the length of detonable region remains at 675 mm. Although the 5000-mm tube length far exceeds the length of most practical PDE tubes, it does provide a clear picture of the effect of the interface expansion waves on the flow development and a limiting case in which the maximum benefit can be obtained from partially filling the tube with air. Figure 9 shows the pressure histories at 0, 337, 675, 1112, 1350 and 2000 mm from the end wall. These locations and, also, the pressure scale in Fig. 9 are chosen to match that in Fig. 8 for the 1350-mm tube with the detonable zone of 675 mm. In the 1350-mm case, the development of the pressure profiles is identical to those at the same locations in the 5000-mm case before the exit expansion waves reach those locations. By comparing Figs. 8 and 9, one can obtain the time at which the exit expansion waves reach a specific location in the shorter (1350-mm) tube. For example, the exit expansion waves reach 675-mm location at about 1.6 ms and the end wall at about 2.8 ms.

In the 1350-mm case, the plateau pressure region at about 6.5 atm is only observed on the pressure histories at 1112 mm. In the 5000-mm case, this plateau region can be seen at any location between the 1000 and 4000 mm from the end wall (Figs. 9 and 10). This observation, consistent with what was observed in the case of 1350-mm tube with a 337-mm detonable section, implies that, given enough time, the interface expansion waves are able to establish this pressure plateau for the reason discussed earlier. There are no pressure plateaus at 6.5 atm observed on pressure histories taken at the exit point in the cases discussed. This is not surprising because the exit region is always under the heavy influence of the exit expansion waves after the shock leaves the tube.

Comparison Between Simulations and Experiments

Figure 11 shows a comparison between the end-wall pressure histories from our simulations and the experiments at Stanford University[17] for a 1350-mm tube filled with the stoichiometric C_2H_4–O_2 mixture with fill lengths of 25, 50, 75, and 100% of tube length. The results of the simulation and experimental data agree

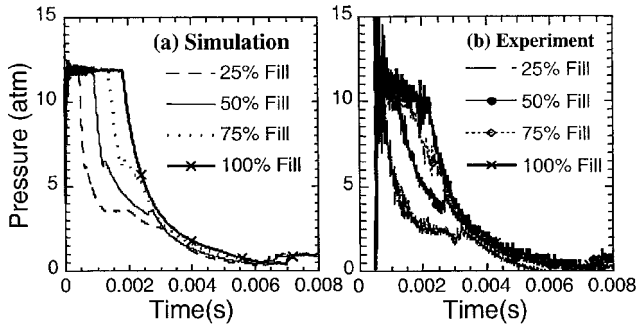

Fig. 11 Comparison of the head-end (thrust wall) pressure histories from a) simulations and b) Stanford experiments.[17]

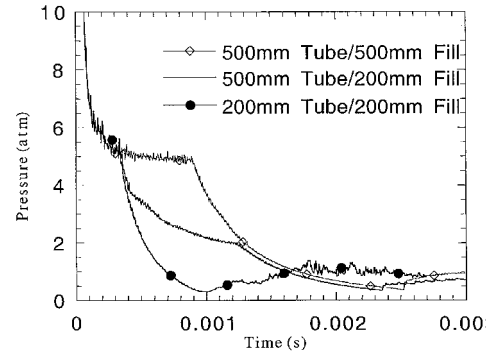

Fig. 12 End-wall pressure histories from the simulations for a 500-mm tube with a 500-mm fuel section, 500-mm tube with with a 200-mm fuel section, and 200-mm tube with a 200-mm fuel section.

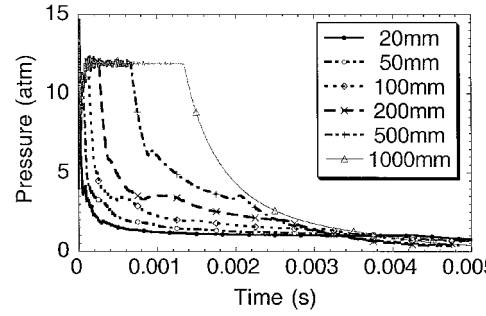

Fig. 13 End-wall pressure histories from the cases of the 1000-mm PDE tube with a fuel section of a different length.

fairly well. The initial pressure spikes are probably due to the specific detonation initiation process used in the experiment. The minor differences in the pressure plateau shape in the fully filled case can probably be attributed to the residual air near the exit. More interestingly, the simulated and experimental pressure histories shown in Fig. 11 are strikingly similar to that observed in our previously reported simulations (Fig. 9 in Ref. 15) for a very different tube length and mixture condition (500-mm tube with an ethylene–air mixture of different fill lengths). This observation implies that the same controlling factors, such as the exit expansion waves and the interface expansion waves, are general features in partially filled PDEs. They affect the flow development in the cases of very different geometric and mixture parameters in a very similar fashion.

Important Factors in Thrust Production

It is evident from the earlier discussion that the flowfield in a partially filled PDE is dominated by three sets of waves: 1) the original detonation and its degenerated form of nonreactive shock, 2) the exit expansion waves, and 3) the interface expansion waves. These waves control the evolution of the pressure distribution on the tube wall and, therefore, the thrust production. In general, total thrust is the time integration of summation of the pressure component in the direction of system motion over the entire tube wall. In the case of the idealized PDE tube considered here, the thrust is proportional to time integration of the pressure history on the end wall. In this section, we will discuss the end-wall pressure histories from several sets of simulations to demonstrate how these pressure waves, especially the interface expansion waves, affect the end-wall pressure and, therefore, the thrust production.

Among all three sets of pressure waves, the detonation is the one that provides the high pressure on the end wall to produce thrust. However, the high pressure generated by the detonation is gradually reduced by the interface expansion and exit expansion waves. Figure 12 shows the end-wall pressure histories from three simulations: 1) a 500-mm tube with a 500-mm fuel section, 2) a 500-mm tube with a 200-mm fuel section, and (3) a 200-mm tube with a 200-mm fuel section. The fuel mixture used in the simulations is C_2H_4:O_2:N_2/1:3:11.28 (stoichiometric ethylene–air mixture). The three pressure histories shown in Fig. 12 clearly demonstrate how the interface expansion waves affect the end-wall pressure and compare to the exit expansion waves. In the case of the 500-mm tube fully filled with fuel, the exit expansion waves arrived at the end wall at about 0.88 ms after detonation initiation. In 200-mm fully filled tube, the exit expansion waves reach the end wall at about 0.37 ms after detonation initiation. The difference in the arrival times corresponds to that for the expansion waves to travel through the difference in the tube length (300 mm) at the local sound speed in the combustion product behind the detonation. In both cases, after the exit expansion reaches the end wall, the pressure is reduced rapidly at a very similar rate. This is consistent with that, in both cases, the detonation goes through a very similar process when it exits the tube and, therefore, produces very similar expansion wave structures.

In the case of the 500-mm tube with a 200-mm fuel section, the interface expansion waves are generated when the detonation passes through the material interface located 200 cm from the end wall. The time needed for the interface expansion to travel to the end wall in this case is very similar to that required by the exit expansion wave in the 200-mm, fully filled tube. Therefore, the interface expansion waves arrive at the end wall at almost the same time (0.37 ms). However, the interface expansion waves are weaker than the exit expansion waves because the shock degenerated from the detonation is still confined in the tube for a significant time after the detonation is quenched. In the 500-mm-tube, 200-mm-fill case, the weaker interface expansion waves result in a slower rate of decline in the end-wall pressure, which gives rise to a higher thrust production than that in the 200-mm-tube, full-fill cases. Because the same amount chemical energy is converted in both cases, the higher thrust means that more converted chemical energy is recovered in the 500-mm-tube, 200-mm-fill case. However, the thrust production is highest in the 500-mm-tube, full-fill case because the converted chemical energy is more than doubled, although a significant part of it is lost through the exit expansion.

Having described the effect of the interface expansion on the end-wall pressure, we now present two sets of simulations that use different ways to change the ratio of tube length to fuel length: 1) a 1000-mm-long PDE tube with the fuel-section length ranging from 20 to 1000 mm and 2) a tube of variable length ranging from 100 to 5000 mm with a fixed fuel-section length of 100 mm. The fill pressure in the tube is 1.0 atm. The fuel section is filled with a stoichiometric ethylene–oxygen mixture (C_2H_4:O_2/1:3), and the rest of tube is filled with air. These two different sets simulations cover wide ranges of tube length and fuel section length.

Figure 13 shows the end-wall pressure histories from the simulations in set 1. In this set, the thrust tube length is 1000 mm and the fuel-section length is 20, 50, 100, 200, 500, and 1000 mm. In all cases, there is a short period in which pressure oscillates due to the detonation initiation process. It can be clearly seen in the cases of 1000-, 500-, and 100-mm fuel length that this initial oscillatory period lasts about 0.2 ms. After this initial period, the pressure on the end wall levels off at about 12 atm. In the fully filled case (1000-mm fuel section), the pressure at the end wall remains at this value until about 1.35 ms after the detonation initiation. At the end of this plateau period, the expansion waves from the tube exit arrive at the

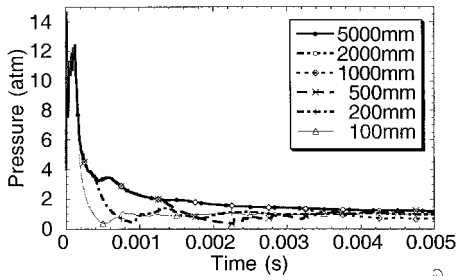

Fig. 14 End-wall pressure histories from the cases of the 100-mm fuel section with a variable tube length.

end wall and begin to reduce the pressure. In the 500- and 200-mm cases, the plateau is significantly shorter than that in the 1000-mm case. In these two cases, the plateau is terminated by the expansion waves generated at the interface at the end of the fuel section, which arrive at the end wall earlier than the exit expansion waves. Time differences in the plateau length between the two partially filled cases and the fully filled case approximately correspond to the time needed for the exit expansion waves to travel through the length of the air section at the sound speed determined by the after-detonation condition. In the 100-, 50-, and 20-mm cases, the filling section is not long enough to establish the pressure plateau before the interface expansion waves arrive at the end wall. In all partially filled cases, the end-wall pressure begins to decrease after the interface expansion waves reach the end wall. Later, the end-wall pressure is further reduced by the exit expansion waves.

Figure 14 shows pressure histories at the end-wall from the simulations in set 2, in which the tube length is 100, 200, 500, 1000, 2000, and 5000 mm while the fuel length is kept at 100 mm. Similar to the cases in set 1, there is an initial oscillatory period due to the detonation initiation process. Because the fuel section is too short, no plateaus are observed in the end-wall pressure histories from all cases simulated in set 2. In the 100-mm tube, which happens to be fully filled with the fuel, the exit expansion waves reach the end wall at about 0.16 ms and the pressure begins to decline. Within 0.48 ms after detonation initiation, the end-wall pressure quickly drops to a subatmospheric level. In all partially filled cases, the interface expansion waves, instead of the exit expansion waves as in 100-mm tube, also arrive at the end wall at about 0.16 ms. After the interface expansion waves reach the end wall, the pressure starts decreasing. Later, the exit expansion waves arrive at the end wall, causing the pressure to reduce at a greater rate. The arrival of the exit expansion waves is marked by a slope change in the pressure history. In the 200-, 500-, and 1000-mm cases, the exit expansion waves reach the end wall at about 0.43, 1.23, and 3.19 ms, respectively. In the 2000- and 5000-mm cases, arrival times of the exit expansion waves are about 6.78 and 17.62 ms, respectively and, hence, are beyond the scale of Fig. 14. In all of these partially filled cases, the fuel section is the same, and the interface expansion waves reach the end wall at the same time. Therefore, in each case, before the exit expansion waves reach the end wall, the pressure development is identical to that in the cases of the longer tube. Also, the inflection point in the pressure history, which marks the arrival of the exit expansion waves, coincides with the time when the pressure history curve deviates from those in the longer tube cases.

Performance Trends

It is evident from the preceding discussion that the interface and exit expansion waves determine the end-wall pressure history for a given detonation strength. The onset and propagation process of these expansion waves are controlled by the length of the tube and the fuel section. Based on the end-wall pressure histories discussed, we can obtain performance data such as the impulse, total-mixture-based specific impulse I_{sp}^{m} and fuel-based specific impulse I_{sp}^{f}, each reflecting different performance characteristics. For the idealized PDE simulated in this study, the impulse can be calculated by integrating the end-wall pressure over time. The impulse reflects the

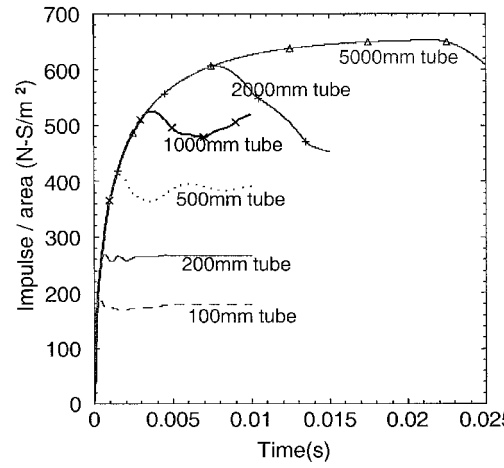

Fig. 15 Impulse development from the cases of the 100-mm fuel section with a variable tube length.

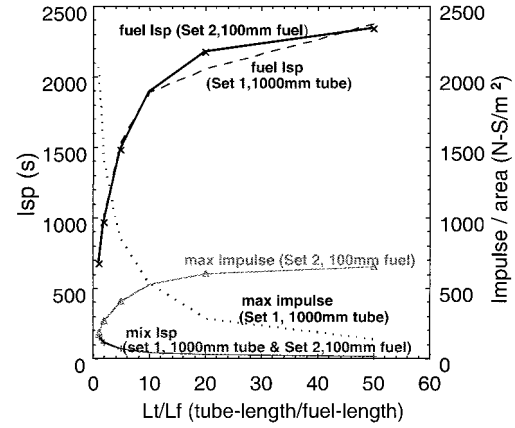

Fig. 16 Maximum impulse, fuel-based I_{sp}, and total-mixture based from set 1, 1000-mm tube with a fuel section of different length, and set 2, 100-mm fuel section in a tube of variable length.

cumulative thrust during an operating cycle, and the averaged thrust can be obtained by dividing the impulse by the cycle time. In each case, the maximum impulse value is reached when the end-wall pressure just becomes sub-atmospheric. Figure 15 shows the impulse per unit area from simulations in set 2. It is evident from Fig. 15 that the longer the tube is, the higher is the maximum impulse value and, also, the later is the time when the maximum impulse is reached. In addition to the tube length, the time for the peak impulse value also depends on the length of the fuel section, the detonation velocity in the unburned mixture, and the sound speed in the burned mixture. This peak time actually can be used as an important factor in determining the time to begin the tube evacuation and refueling process.

For a PDE, there are two ways to define the specific impulse I_{sp}: total-mixture-based specific impulse I_{sp}^{m} and fuel-based specific impulse I_{sp}^{f}. I_{sp}^{m} represents the fuel efficiency of a rocket-like propulsion system where both fuel and oxidizer are carried in the system. I_{sp}^{f} reflects the fuel efficiency of an airbreathing propulsion system where only the fuel is carried onboard and the oxidizer is taken from the ambient environment. Presently, PDE is considered for both airbreathing and pulse detonation rocket engine (PDRE) applications, and a proper I_{sp} should be used to evaluate the fuel efficiency depending on the specific application.

Figure 16 shows the maximum impulse per unit area as a function of the ratio of the tube length to the fuel-section length (L_t/L_f) from both sets of simulations. In cases simulated in set 1, the maximum impulse has the highest value at $L_t/L_f = 1$, and it decreases as L_t/L_f increases. This is because in set 1 cases with the fixed tube length the length of the fuel section, and, therefore, the total chemical energy

content in the tube, is lower for a larger L_t/L_f due to a shorter fuel section. Also, because the density difference between the fuel mixture and air is quite small, the total mass of the gaseous content in the fuel and air section in the fixed length tube considered in set 1 does not change much. Therefore, I_{sp}^m for the cases in set 1 follows a similar trend to that of the maximum impulse.

For the cases in set 2, the trend in the peak impulse is reversed from that for the cases in set 1. In set 2, the fuel-section length is fixed and, therefore, so is the total chemical energy content in the PDE tubes of different lengths. Because a longer tube is favorable for retaining the high pressure in the tube, the maximum impulse goes up as L_t/L_f increases due to a longer tube. However, the total mass of the mixtures in tube increases at a rate approximately proportional to the tube length. The increase in the total mixture mass outweighs the increase in the maximum impulse as the L_t/L_f increase with the tube length. As a consequence, for cases in set 2, I_{sp}^m reduces as L_t/L_f increases.

Note that the two I_{sp}^m curves, as functions of L_t/L_f, from the two different sets of simulations converge together. This means that the impulse produced by a unit total mixture in PDEs of different length is the same so long as the L_t/L_f remains identical. A more interesting feature shown in Fig. 16 is the fuel-based specific impulse I_{sp}^f. Similar to I_{sp}^m, for the cases simulated in the two sets, the two I_{sp}^f curves representing the two different sets are very close together. This means that, in a wide range of lengths of the tube and fuel section, I_{sp}^f scales with L_t/L_f. As the L_t/L_f increases due to either increase in the tube length or decrease in the fuel-section length, I_{sp}^f increases. Starting from $L_t/L_f = 1.0$, I_{sp}^f increases rapidly initially and, then, gradually levels off at a level just below 2500 s. Figure 16 also shows that about 80% of the maximum I_{sp}^f can be achieved with a ratio of $L_t/L_f = 10$.

The scaling relationship between I_{sp}^f and L_t/L_f provides an important trend in the fuel efficiency for PDE applications in airbreathing propulsion. Because the amount of chemical energy is fixed for a given amount fuel, it is conceivable that, as L_t/L_f increases, the fuel-based specific impulse I_{sp}^f asymptotically approaches a limiting value. From the simulated cases, this asymptotical limit is likely to be around 2500 s. Furthermore, the ratio of I_{sp}^f of a partially filled PDE to that of a fully filled one can be expressed by the following fitting formula:

$$I_{sp}^f \Big/ I_{sp\,\text{fully-filled}}^f = \boldsymbol{a} - (\boldsymbol{a} - 1)/\exp\{(L_t/L_f - 1)/8\}$$

where the constant $\boldsymbol{a}$ is the asymptotic limit of the benefit multiplier, representing the maximum benefit that can be obtained by using partial fuel filling. For the simulated cases, the constant $\boldsymbol{a}$ has a value ranging from 3.2 to 3.5. For a given L_t/L_f, the difference between the value calculated from this fitting formula and that from the simulations is less than 10%. For the extension tubes of 7–10 times of the fuel section presented in Ref. 6, assuming $\boldsymbol{a} = 3.2$, $I_{sp}^f/I_{sp\,\text{fully-filled}}^f$ has an estimated value ranging from 2.05 to 2.48 from the fitting formula, which is in a reasonable agreement with the experimental observation (about 2 for the entire range of the tube length from 7 to 10) from Ref. 6, when the experimental uncertainty is considered.

Summary

Comprehensive analysis for the partial fuel filling process was conducted based on systematic numerical simulations of the development of the flowfield during the PDE cycle. In a PDE partially filled with a combustible mixture, the flowfield is dominated by three sets of pressure waves: 1) the detonation, 2) the interface expansion waves generated at the material interface between the combustible and nonreactive sections, and 3) the exit expansion waves generated when the detonation exits the tube. For a detonation of a given strength (determined by the mixture condition), the interface and exit expansion waves control the evolution of the pressure distribution in the tube and, therefore, the thrust production. The onset and propagation process of those expansion waves are, in turn, determined by the length of the PDE tube and the fuel section. The analysis further shows that the fuel-based specific impulse I_{sp}^f increases with L_t/L_f. On the other hand, the total-mixture-based specific impulse I_{sp}^m declines as L_t/L_f increases.

The benefit of partial fuel filling depends on the specific application. For airbreathing applications, the fuel-based specific impulse I_{sp}^f reflects the fuel efficiency of the system. For the studied cases, I_{sp}^f can be uniquely determined for each L_t/L_f value and improves as L_t/L_f increases. However, the rate of increase in I_{sp}^f gradually slows down, and improvement in the fuel efficiency diminishes as L_t/L_f becomes very large (over 10). Also, in PDE design, other performance criteria such as required average thrust, that is, the total cycle impulse, may have to take precedence over the fuel efficiency. Furthermore, the preceding analysis on fuel efficiency is based on an idealized PDE in which only the weight of the filling mixture (in fuel and air sections) is considered. For a more realistic system, this analysis needs to be modified to include the system weight. For PDRE applications, the total-mass-based impulse I_{sp}^m represents the fuel efficiency and has its maximum value at the minimum L_t/L_f (1.0). Therefore, partial filling is not beneficial at all. This is readily understandable because a rocket system carries all fuel components including both fuel and oxidizer, and therefore, maximum energy content is desirable.

Acknowledgments

This work has been sponsored by the Office of Naval Research through the Mechanics and Energy Conversion Division and the Naval Research Laboratory. A part of the computer time used in this study was provided by the Department of Defense High-Performance Computing Center at the Naval Research Laboratory.

References

[1]Nicholls, J. A., Wilkinson, H. R., and Morrison, R. B., "Intermittent Detonation as a Thrust-Producing Mechanism," *Jet Propulsion*, Vol. 27, No. 5, 1957, pp. 534–541.

[2]Eidelman, S., and Grossmann, W., "Pulse Detonation Engine: Experimental and Theoretical Review," AIAA Paper 92-3168, July 1992.

[3]Bussing, T., and Pappas, G., "Introduction to Pulse Detonation Engine," AIAA Paper 94-0263, Jan. 1994.

[4]Kailasanath, K., "Applications of Detonations to Propulsion: A Review," *AIAA Journal*, Vol. 38, No. 4, 2000, pp. 1698–1708.

[5]Kailasanath, K., "Recent Developments in the Research on Pulse Detonations Engines," *AIAA Journal*, Vol. 41, No. 2, 2003, pp. 145–159.

[6]Zhdan, S. A., Mitrofanov, V. V., and Sychev, A. I., "Reactive Impulse from the Explosion of a Gas Mixture in a Semi-Infinite Space," *Explosion and Shock Waves*, Vol. 30, No. 5, 1994, pp. 657–663.

[7]Zitoun, R., Gamezo, V., Guerraud, C., and Desbordes, D., "Experimental Study on the Propulsive Efficiency of Pulsed Detonation," *Proceedings of the 21th International Symposium on Shock Waves*, Paper 8292, July 1997.

[8]Eidelman, S., and Yang, X., "Analysis of the Pulse Detonation Engine Efficiency," AIAA Paper 98-3877, July 1998.

[9]Falempin, F., Bouchard, D., and Daniau, E., "Pulsed Detonation Engine: Towards a Tactical Missile Application," AIAA Paper 2000-3473, July 2000.

[10]Mohanraj, R., and Merkle, C. L., "Numerical Study of Pulse Detonation Engine Performance," AIAA Paper 2002-0315, Jan. 2000.

[11]Zitoun, R., and Desbordes, D., "Propulsive Performances of Pulsed Detonations," *Combustion Science and Technology*, Vol. 144, No. 1, 2001, pp. 93–114.

[12]Falempin, F., Bouchard, D., Forrat, D., Desbordes, D., and Daniau, E., "Pulsed Detonation Engine: Possible Application to Low Cost Tactical Missile and to Space Launcher," AIAA Paper 2001-3812, July 2001.

[13]Daniau, E., Zitoun, R., and Desbordes, D., "Effects of Nozzles of Different Length and Shape on Propulsive Performance of Pulse Detonation Engine," *High-Speed Deflagration and Detonation: Fundamentals and Control*, edited by G. D. Roy, S. M. Frolov, D. W. Netzer, and A. A. Borisov, ELEX-KM Publishers, Moscow 2001, pp. 251–262.

[14]Cambier, J. L., and Tegner, J. K., "Strategies for PDE Performance Optimization," AIAA Paper 97-2743, July 1997.

[15]Li, C., and Kailasanath, K., "A Numerical Study of Flow Field Evolution in Pulse Detonation Engines," AIAA Paper 2000-0314, Jan. 2000.

[16]Brophy, C. M., Sinibaldi, J., and Netzer, D. W., "Effects of Fuel Distribution on Pulse Detonation Engine Operation and Performance," International Symposium on Air Breathing Engines, Paper ISABE-2001-1173, Sept. 2001.

[17]Sanders, S. T., Jenkins, T. P., and Hanson R. K., "Diode-Laser Sensor System for Multi-Parameter Measurements in Pulse Detonation Engine Flows," AIAA Paper 2000-3592, July 2000.

[18]Jenkins, T. P., Sanders, S. T., Kailasanath, K., Li, C., and Hanson, R. D., "Diode-Laser Based Measurements for Model Validation in Pulse Detonation Flows," CPIA Vol. 701, Chemical Propulsion Information Agency, Laurel, MD, 2000, pp. 422–430.

[19]Boris, J. P., and Book, D. L., "Flux-Corrected Transport I: SHASTA, A Fluid Transport Algorithm that Works," *Journal of Computational Physics*, Vol. 11, No. 1, 1973, pp. 38–46.

[20]Boris, J. P., Landsberg, A. M., Oran, E. S., and Gardner, J. H., "LCPFCT—A Flux-Corrected Transport Algorithm for Solving Generalized Continuity Equations," U.S. Naval Research Lab., NRL Memorandum Rept. 6410-93-7192, Washington, DC, 1993.

[21]Li, C., Kailasanath, K., and Oran, E. S., "Detonation Structure behind Oblique Shocks," *Physics of Fluids*, Vol. 6, No. 4, 1994, pp. 1600–1611.

[22]Babushok, V. I., and Dakdancha., A. N., "Globe Kinetic Parameters for High-Temperature Gas-Phase Reactions," *Combustion, Explosion and Shock Waves*, Vol. 29, No. 4, 1993, pp. 48–80.

[23]Oran, E. S., and Boris, J. P., *Numerical Simulation of Reactive Flow*, Elsevier, New York, 1987.

[24]Stull, D. R., and Prophet, H., *JANNAF Thermochemical Tables*, 2nd ed., National Bureau of Standards, Washington, DC, 1972.

[25]Gorden, S., and McBride B. J., "Computer Program for Calculations of Complex Chemical Equilibrium Compositions, Rocket Performance, Incident and Reflected Shocks, and Chapman-Jouguet Detonations," NASA SP-273, 1976.